Molecular Sieving of Propyne/Propylene by a Scalable Nanoporous Crystal with Confined Rotational Shutters

Wan, J.; Zhou, H.-L.; Hyeon-Deuk, K.; Chang, I.-Y.; Huang, Y.; Krishna, R.; Duan, J.

DOI
10.1002/ange.202316792
10.1002/anie.202316792

Publication date
2023

Document Version
Final published version

Published in
Angewandte Chemie

Zitierweise: *Angew. Chem. Int. Ed.* **2023**, *62*, e202316792
doi.org/10.1002/anie.202316792

Gas Separation

Molecular Sieving of Propyne/Propylene by a Scalable Nanoporous Crystal with Confined Rotational Shutters

*Jingmeng Wan, Hao-Long Zhou, Kim Hyeon-Deuk, I-Ya Chang, Yuhang Huang, Rajamani Krishna, and Jingui Duan**

Abstract: Soft porous coordination polymers (PCPs) have the remarkable ability to recognize similar molecules as a result of their structural dynamics. However, their guest-induced gate-opening behaviors often lead to issues with selectivity and separation efficiency, as co-adsorption is nearly unavoidable. Herein, we report a strategy of a confined-rotational shutter, in which the rotation of pyridyl rings within the confined nanospace of a halogen-bonded coordination framework (**NTU-88**) creates a maximum aperture of 4.4 Å, which is very close to the molecular size of propyne (C_3H_4: 4.4 Å), but smaller than that of propylene (C_3H_6: 5.4 Å). This has been evidenced by crystallographic analyses and modelling calculations. The **NTU-88o** (open phase of activated **NTU-88**) demonstrates dedicated C_3H_4 adsorption, and thereby leads to a sieving separation of C_3H_4/C_3H_6 under ambient conditions. The integrated nature of high uptake ratio, considerable capacity, scalable synthesis, and good stability make **NTU-88** a promising candidate for the feasible removal of C_3H_4 from C_3H_4/C_3H_6 mixtures. In principle, this strategy holds high potential for extension to soft families, making it a powerful tool for optimizing materials that can tackle challenging separations with no co-adsorption, while retaining the crucial aspect of high capacity.

Introduction

The chemical industry heavily relies on distillation or catalytic conversion to separate chemicals into their pure forms, particularly small gases.[1] However, this accounts for a quarter of the world's energy consumption, making it imperative to develop transitional or alternative technologies that are highly efficient, energy-saving, and low-cost. One promising technology is physio-adsorption in porous materials, which has the potential to reduce energy intensity by a factor of 10 or more. This non-thermal technology has already been successfully used in oxygen/nitrogen separation using ZMS zeolites.[2–3] However, the current and major hurdle still exists in the industry, such as the deep removal of C_3H_4 from C_3H_6, a main and large quantity raw material for the production of value-added chemicals. This is due to the fact that two molecules have very similar structure and molecular sizes (C_3H_4: 4.4×6.8 Å^2, C_3H_6: 5.4×6.8 Å^2), in addition to the low concentration of C_3H_4 (usually up to 3.6 % in companies, China) in the mixtures.[4–7]

Porous materials, specifically porous coordination polymers (PCPs), also called metal–organic frameworks, are a new type of crystalline porous materials that have shown a great potential to be used in nanopore chemistry for separation applications.[8–16] These materials possess inherent modularity and can be easily designed, making them highly suitable for energy-efficient gas recognition and accommodation. However, to establish a more effective adsorbent, the sieving properties of PCPs should be considered firstly, exemplified by the rigid frameworks of KAUST-7 (C_3H_6/C_3H_8 splitter) and the UTSA-280 (C_2H_4/C_2H_6 sieve).[17–18] Notably, there are significant challenges in designing and constructing rigid pores with perfect size/shape for sieving C_3H_4/C_3H_6 mixtures, especially considering the more or less inherent flexibility of coordinated porous frameworks.

Comparably, soft PCPs, an unique class of porous materials that exhibit stimulus-responsive phase transformations, have been considered as one of the most exciting discoveries in recent.[19–27] These materials can be designed to be sensitive to different guests, but, co-adsorption is a common challenge once the pore was opened. Therefore, we here believe that the strategy of confined-rotational shutters is expected to break through this limitation, as the confined space within the micro-porous framework (2.5–4.0 Å) determines the trajectory of the rotating unit, allowing structural changes under external stimuli to meet the requirements for molecular sieving of these two similar molecules. This approach will effectively prevents co-adsorption, which usually occurs in other soft frameworks due to random or significant changes. Although soft PCPs, including layer sliding, framework distortion, flexible nodes or dynamic gating, have been extensively reported,[28–32] the challenge

[*] J. Wan, Y. Huang, Prof. Dr. J. Duan
State Key Laboratory of Materials-Oriented Chemical Engineering, College of Chemical Engineering, Nanjing Tech University
211816 Nanjing (China)
E-mail: duanjingui@njtech.edu.cn
Prof. Dr. H.-L. Zhou
Department of Chemistry, Shantou University
515063 Shantou (China)
Prof. Dr. K. Hyeon-Deuk, Dr. I-Y. Chang
Department of Chemistry, Kyoto University
606-8502 Kyoto (Japan)
Prof. Dr. R. Krishna
Van 't Hoff Institute for Molecular Sciences, University of Amsterdam
Science Park 904, 1098 XH Amsterdam (The Netherlands)

remains in achieving an open phase that can effectively prevent co-adsorption of gas pairs with extremely similar properties, while still maintaining a high adsorption capacity for the recognized molecule.[27,33]

During our exploration in soft materials,[18,33–34] we recently developed a confined strategy involving the use of water nanotubes within a robust framework. Thanks to the protection provided by this framework, the confined water nanotubes exhibited exclusive adsorption of C_3H_6, but not C_3H_8. However, the lower porosity of the water nanotubes has motivated us to develop a new system. In this work, we report a strategy of confined-rotational shutters (Scheme 1), where the rotation of pyridyl rings from the ligand (**L**: 4,4′-dipyridylnitride) in the nanospace of a halogen-bonded framework boosts the sieving separation of C_3H_4/C_3H_6 mixtures. Furthermore, the accurate identification of gas-induced transition structures provides valuable insights into the separation mechanism at the molecular-level.

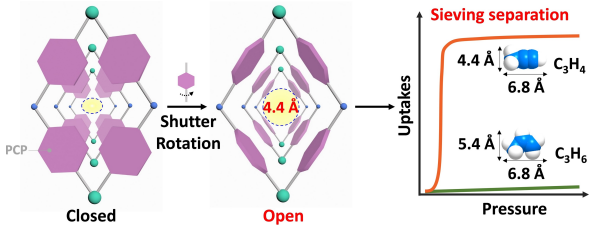

Scheme 1. Illustration of the confined-rotational shutters strategy in micro-porous crystals for sieving of C_3H_4/C_3H_6 mixtures by eliminating co-adsorption.

Results and Discussion

Green rhombus-shaped crystals (**NTU-88**) were obtained through a solvothermal reaction of 4, 4′-dipyridylnitride (**L**) and $NiCl_2 \cdot 6H_2O$ in *N,N′*-dimethylformamide/ethanol/H_2O. Single-crystal X-ray diffraction (SCXRD) structural analysis revealed that it crystallizes in the orthorhombic system with *P*bcn space group (Table S1).[35] The asymmetric unit consists of half a Ni^{2+} cation, one Cl^- anion, and one ligand, giving the formula $[Ni(\mathbf{L})_2Cl_2]\cdot x$Solvent for **NTU-88**. Each ligand is connected to two Ni ions, while, four N atoms from four ligands and two charge balanced Cl^- anions complete the coordination geometry of the mononuclear nickel node (Figure S2). Therefore, a typical **sql** layer with a rhombus pore of 5.3×8.8 $Å^2$ was established. In addition, with a side length of 11.232 Å, the angle of ∠Ni–Ni–Ni in the rhombus pore is 108.87° (Figure 1a). The adjacent AB layers are stacked together through the formation of relatively strong hydrogen bonds ($d_{Cl\cdots H-N}$: 2.363 Å), creating a supramolecular structure. Additionally, the two coordinated Cl atoms form hydrogen bonds with the H atoms from the four pyridine rings (Figure S3–S4 and Table S2), resulting in a restricted configuration of the pyridine rings (dihedral angle: 55.41°) in the V-shaped ligand. Additionally, the substantial rhombus pore present in the single layer has been tailored into a one-dimensional (1D) zigzag channel (3.2×5.6 $Å^2$) within the packed frameworks (Figure 1b–1c).

The structures and phase purities of the as-synthesized **NTU-88** were confirmed by PXRD analysis (Figure S7). After exchanging the guest with dry methanol, the fully activated **NTU-88** was obtained by degassing under high vacuum at 373 K according to the thermogravimetric (TG) results (Figure S8). However, the diffraction pattern of the desolated crystals (**NTU-88c**) was different, indicating a structural transformation. Based on this pattern, the structure of **NTU-88c** was established by Pawley refinement

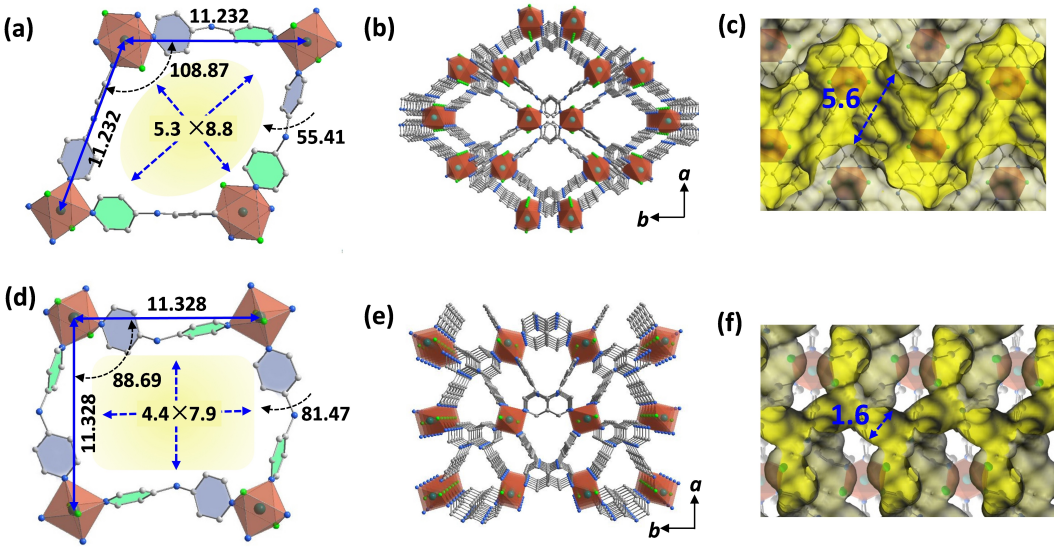

Figure 1. Structural comparison: Single-layer (a), multi-layers (b) and accessible inner pore (c) of **NTU-88**; Single-layer (d), multi-layers (e) and accessible inner pore (f) of **NTU-88c**. Units for distances and angles are Å and °, respectively.

(Figure S10 and Table S3). The crystal system changed to monoclinic with a $P2_1/c$ space group. Although the coordination connections of the metal node and organic linker remained the same as before, the configuration of the pore in the single layer underwent a significant change. The initial rhombus pore changed into a nearly rectangular one (4.4×7.9 Å^2) with an angle of ∠Ni–Ni–Ni of 88.69°. In addition, a rotation occurred on the pyridine ring, giving a dihedral angle of 81.47°. Meanwhile, the initial accessible pore in **NTU-88** was tailored into a state with a very tiny pore (1.6 Å) (Figure 1d–1f).

Considering the framework change after activation, it was expected that the framework of **NTU-88c** would undergo structural changes during gas adsorption. The permanent porosity of **NTU-88c** was analysed by CO_2 (195 K) and N_2 (77 K) adsorption isotherms (Figure 2a). Negligible N_2, but significant CO_2 uptake, were observed. The adsorption of CO_2 can be divided into two stages: a gradual increase before reaching $P/P_0=0.015$ followed by a sudden increase. Based on the CO_2 adsorption isotherm, the Brunauer–Emmett–Teller (BET) surface area was calculated to be $\approx420\ m^2\cdot g^{-1}$. Giving this observation, single-component adsorption isotherm of C_3H_4 was collected at 298 K (Figure 2b). Similarly, the isotherm showed a two-step adsorption process, with a rapid uptake occurring at about 15.6 kPa. Further, in situ PXRD analysis during the adsorption-desorption process revealed a notable phenomenon. The peaks corresponding to the [−1 1 1] and [0 3 1] planes exhibit a gradually shifted to a lower angle as the pressure initially increased, indicating a slight expansion of the *AB*-layers and the angle of the V-shaped ligand. Interestingly, the peaks associated with the [1 0 0] and [−1 1 1] crystal planes merged into a single peak at about $2\theta=11.1°$, showing the formation of a new phase (Figure 2c and S11–S12). This significant change is consistent with the sudden C_3H_4 uptake. In addition, the PXRD patterns did not show any observable changes until the pressure decreased to 10 kPa. Interestingly, when the pressure decreased to 5 kPa, the merged peak splits into two, with positions consistent with that of **NTU-88c**, indicating the reversibility of structural changes.[29] On the contrary, the PXRD patterns under a C_3H_6 atmosphere did not show any changes throughout the pressure range (Figure 2d and S13).

To explore the reason for the significant differences observed, structural models have been established based on the in situ PXRD data at three representative pressure (8 kPa: **NTU-88α**, 14 kPa: **NTU-88β** and 100 kPa: **NTU-88o**) for C_3H_4 (Figure S10, S14–S15). A comparison of the structures of **NTU-88c**, **NTU-88α** and **NTU-88β** revealed only minor structural change. However, as the pressure increased, there was a gradual increase in the angle of ∠Ni–Ni–Ni in the rhombus pore, from 88.69° up to 89.22°, as well as an increase in the distance between metal nodes (from 11.328 Å to 11.366 Å). Additionally, the pore size of the packed framework also exhibited a slightly increase, from 1.60 to 1.67 Å, as the pyridine rings of the pore wall in these three states were all parallel to the *c*-axis (Figure 3a–3f). Sharply in contrast, a rotation of the pyridine rings in **L** was observed in **NTU-88o**, and the corresponding dihedral angle decreased from 81.38–81.54° in **NTU-88α** and **NTU-88β** to 55.62°. In addition, further sliding and expansion of the adjacent layers yield an enlarged pore size of the

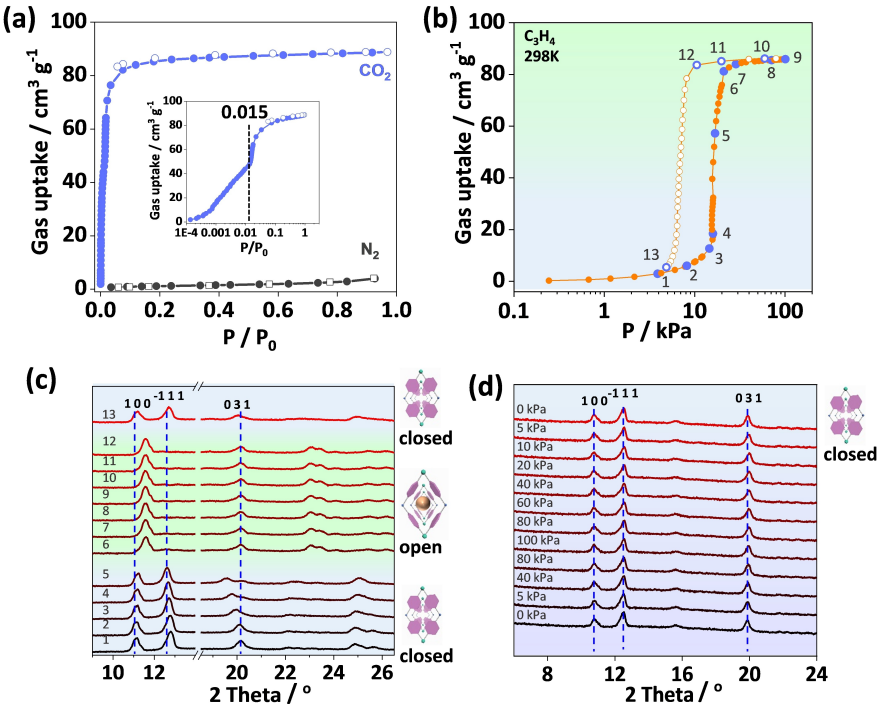

Figure 2. CO_2 (195 K) and N_2 (77 K) adsorption isotherms of **NTU-88** (a); C_3H_4 adsorption isotherm ((b), 298 K) of **NTU-88** and corresponding in-situ XRD during adsorption (c); In-situ XRD of **NTU-88** under C_3H_6 (d). All PXRD patterns were collected at 298 K.

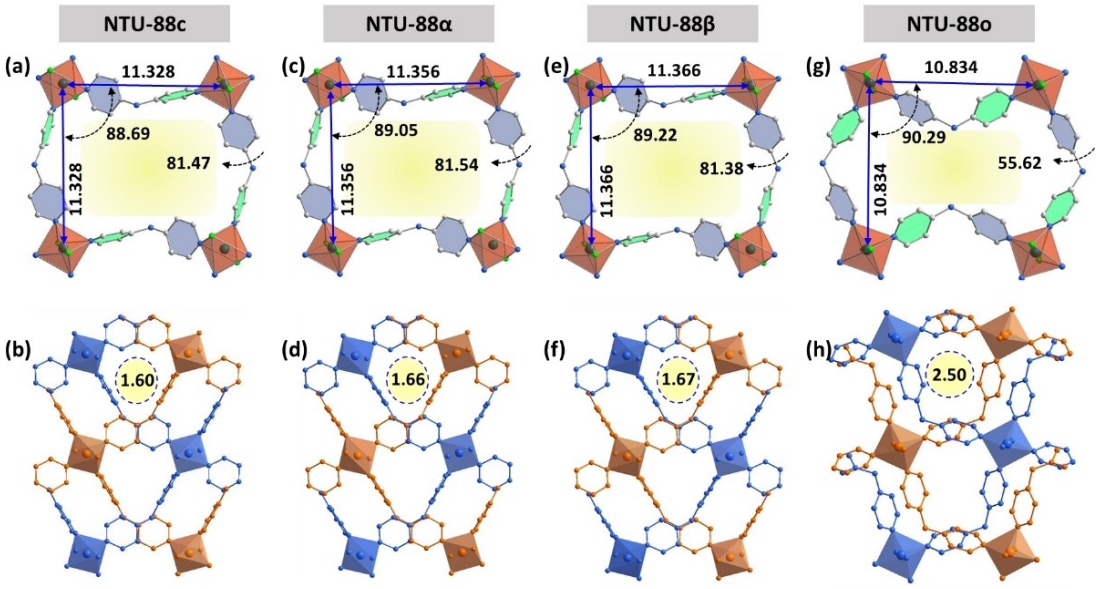

Figure 3. Structural views of **NTU-88** in different states: closed phase of **NTU-88c** (a, b); phase **α** under C_3H_4 at 8 kPa (c, d); phase **β** under C_3H_4 at 14 kPa (e, f); open phase of **NTU-88o** under C_3H_4 at 100 kPa (g, h). The corresponding temperature for all phases is 298 K. Units for distances and angles are Å and °, respectively.

packed layers, of about 2.5 Å (Figure 3g–3 h, S16–S17). Taking the molecular size of C_3H_4 in mind, this relatively small aperture would not allow for a large amount of C_3H_4 adsorption.

To elucidate this phenomenon, density functional theory computations were performed. First, we calculated the electronic density surface to estimate the van der Waals radii of the static pores in the gas channels of **NTU-88c** and **NTU-88o**. The diameters of the narrowest pores of the gas channels, 1.6 Å in **NTU-88c** and 2.5 Å in **NTU-88o**, are too short for both C_3H_4 and C_3H_6 to pass through (Figure 4a–4d). Even the diameters of the broadest pores, 2.4 Å in **NTU-88c** and 3.2 Å in **NTU-88o**, are still shorter than the shortest diameter of C_3H_4 (4.4 Å) and C_3H_6 (5.4 Å) (Figure S18–S19). Therefore, the electronic density surfaces based on the static structures cannot rationalize the present gas sieving. By introducing the rotation of the pyridine rings, we estimated the largest dynamic pore size, which occurs when the faces of the pyridine rings are almost parallel to the *c*-axis, minimizing steric hindrance for gas flow (Figure S20). The diameter of the broadest dynamic pore in **NTU-88c** is still only 3.4 Å, indicating that neither C_3H_4 nor C_3H_6 can pass through **NTU-88c** even with the rotation of pyridine rings (Figure 4e). In contrast, the diameter of the largest dynamic pore in **NTU-88o** is 4.4 Å, which is quite close to the diameter of C_3H_4 but still shorter than the diameter of C_3H_6 (Figure 4f). This means that while C_3H_6 cannot pass through this path in **NTU-88o**, but C_3H_4 can. Therefore, the pyridyl rings in the defined channel in **NTU-88** can be regarded as a confined-rotational shutter, playing a crucial role in the exclusive C_3H_4 adsorption.

The plausible confined-rotational shutter inspired us to explore the adsorption behaviors of C_3H_4 and C_3H_6 on **NTU-88**. The adsorption isotherms of C_3H_4 and C_3H_6 were collected at ambient temperatures and the results showed that the C_3H_4 uptake is as high as 86.0 $cm^3 \cdot g^{-1}$ at 1 bar, 298 K. Interestingly, the maximum uptakes are similar in the temperate range of 273 to 328 K, with only an advanced or delayed pressure for the shutter to open. As expected, C_3H_6 was nearly not adsorbed by **NTU-88** at these temperatures, as its molecular size is larger than the aperture size of **NTU-88o** (4.4 Å: shutter opening) (Figure 5a, S21–S23). Therefore, the results here suggest that the confined-rotational shutter strategy shows great promise in suppressing the co-adsorption of gas pairs with extremely similar properties, a common issue in non-restricted soft frameworks.

The significant differences in adsorption isotherms between C_3H_4 and C_3H_6 make **NTU-88o** stand out among all reported PCPs, with a maximum value of 52.7 (100/100 kPa, 298 K), and it remains almost as a constant (57.1) until the partial pressure of C_3H_4 drops below 20 kPa. In addition, the temperature-dependent shutter opening allows for a high uptake ratio of C_3H_4/C_3H_6, reaching (34.5, 4/96 kPa) at 273 K, which is also the highest among all porous materials. However, the uptake ratio is low at 1 kPa/99 kPa, 298 K, as the rotation of pyridyl rings not occurs at this condition (Figure 5b, S24–S27 and table S4).

To better understand this observation, a structural analysis of C_3H_4-loaded **NTU-88o** was performed (Figure S28–S29). The C_3H_4 molecules were found to be accommodated in the nano-channels of **NTU-88o**. Different with the open shutter in dynamic calculation, the pyridine rings rotate back and form a closed accommodation for C_3H_4 storage. In addition, the C_3H_4 molecules form a compacted and ordered 1D molecular array in the nano-channel. More interestingly, each C_3H_4 molecule forms six hydrogen bonds with adjacent carbons from the pyridine rings, with distance ranging from 2.731–2.921 Å (Figure 5c–

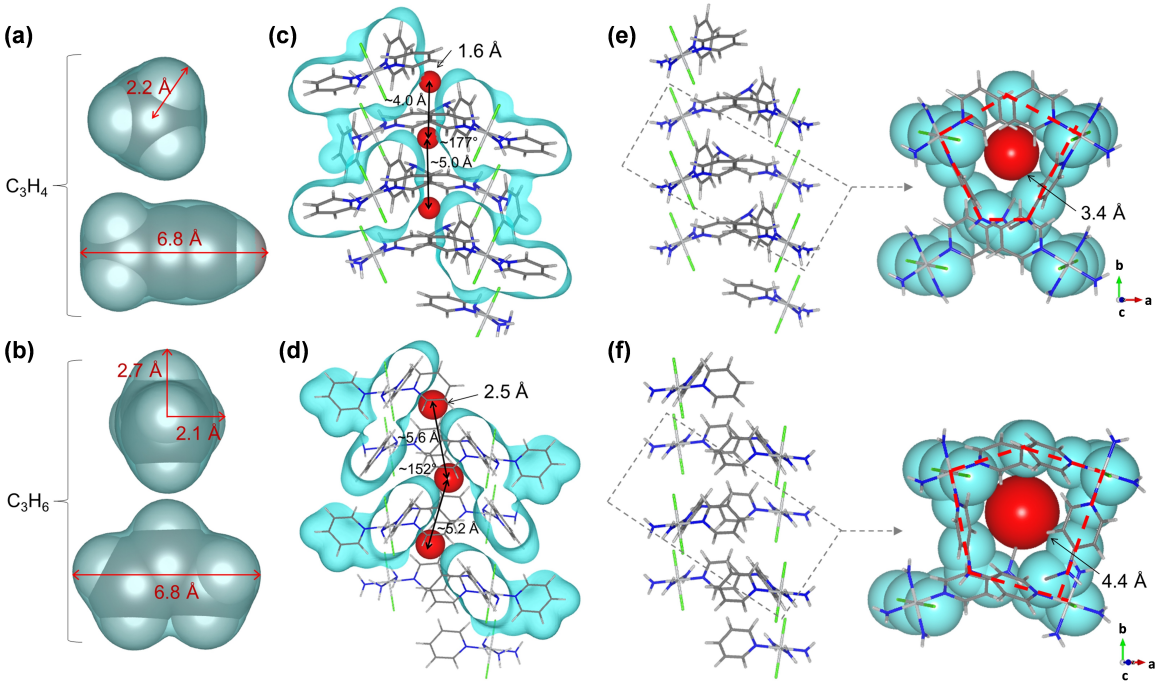

Figure 4. Effective size of C_3H_4 (a) and C_3H_6 (b); static channels existing in **NTU-88c** (c) and **NTU-88o** (d); dynamic channels appearing in **NTU-88c** (e) and **NTU-88o** (f) when the faces of the pyridine rings become almost parallel to the *c*-axis. The red dashed lines in (e, f) describe the pore boundary composed of the Ni atoms as well as the C and N atoms on the rotational axials of the pyridine rings. The light blue regions express the van der Waals radii that determine the effective pore size. The red balls indicate the effective pore size.

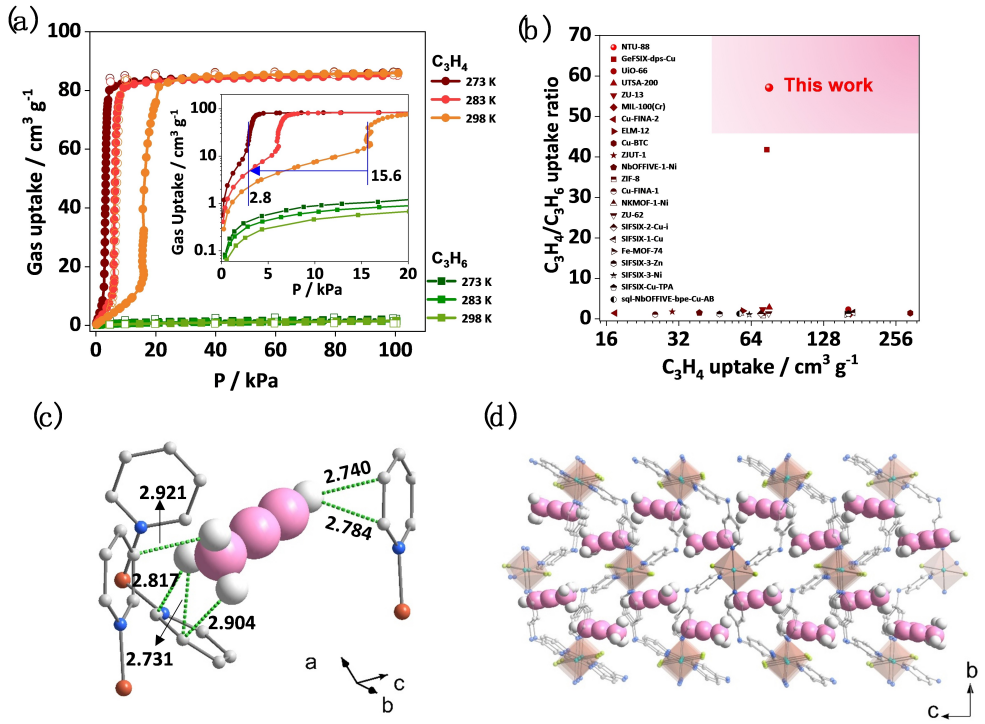

Figure 5. C_3H_4 and C_3H_6 adsorption isotherms of **NTU-88** (a), with the inset showing the re-arranged isotherms at 0–20 kPa; comparison of the C_3H_4/C_3H_6 uptake ratio (20/80 kPa, 298 K) between **NTU-88** and other materials (Table S4) (b); views of the hydrogen bonds of C_3H_4 in **NTU-88o** (c) and C_3H_4 array in **NTU-88o** (d). The gas-loaded crystal analysis was performed at 298 K.

5d). Particularly, the distances of two $\mathbf{C}_{\text{pyridine}}\cdots\mathbf{H}\text{–}\mathbf{C}_{\text{alkyne}}$ bonds are slightly shorter than the sum of the van der Waals radii of the H (1.11 Å) and C (1.72 Å) atoms, reflecting strong host-C_3H_4 interactions, as confirmed further by the relative higher isosteric heat (29.4–44.0 kJ/mol) of adsorption for C_3H_4 (Figure S30–S33, Table S5). Therefore, it is clear that the C_3H_4 molecule, due to its smaller size and stronger interactions with the framework, can open the closed shutters and achieve remarkable adsorption, whereas, the C_3H_6 molecule, being larger in molecular size and having weaker host–guest interactions, is unable to enter the framework throughout the pressure from 0—100–0 kPa at temperature range of 273 to 328 K.

Encouraged by the functions of the confined-rotational shutter, separation ability of **NTU-88** for C_3H_4/C_3H_6 mixtures was evaluated by breakthrough experiments (Figure S34–S42). After introducing an equlimolar feed gas (v/v, 1/1, 2 mL·min^{-1}) into the sample bed, polymer-grade C_3H_6 (99.95 %) elutes out at 11 min and continuing until 49 min at 298 K (Figure 6a). By changing the feed gas to C_3H_4/He (v/v, 1/1, 2 mL·min^{-1}), the curve for C_3H_4 is almost identical to that of the feed gas of C_3H_4/C_3H_6, providing conclusive evidence of complete inhibition of co-adsorption between C_3H_4 and C_3H_6 in **NTU-88**. In addition, the presence of C_3H_8 had a negligible effect on the inhibition of co-adsorption (Figure S43–S44). To further explore the function of the shutter at low C_3H_4 partial pressure, C_3H_4/C_3H_6 mixtures with a changed ratio (v/v, 1/99) were then tested. The breakthrough point for C_3H_6 was similar to that of the feed gas with an equimolar mixture, while the retention time of C_3H_4 extends to 104 min. However, it has been observed that as the velocity of the feed gas increased, the breakthrough points for C_3H_6 occurred earlier, along with the early elution of C_3H_4, (Figure 6b). Interestingly, the capacity for captured C_3H_4 remained almost unchanged at different velocities (10 mL·min^{-1}: 1.50 mL; 5 mL·min^{-1}: 1.53 mL; 2 mL·min^{-1}: 1.60 mL; 1 mL·min^{-1}: 1.63 mL), indicating that the gas speed had a negligible influence on the shutter rotation. Furthermore, during the time interval between C_3H_4 and C_3H_6 breakthrough, the high-purity C_3H_6 productivity (>99.95 %) of **NTU-88** from the outlet effluent was estimated to be 2.42 mmol·g^{-1} (298 K), which was sharply improved by reducing the temperature (4.10 mmol·g^{-1}, 271 K, Figure S42). To validate the exclusive C_3H_4 capture, desorption of the breakthrough experiment was collected. The saturated sample bed was swept with flowing N_2 (5 mL·min^{-1}) until no C_3H_6 is detected. The samples bed was then rapidly heated to 373 K, resulting in the elution of highly pure of C_3H_4 (99.95 %) (Figure S37), showing the positive effect of the confined-rotational shutter in C_3H_4 storage. Thanks to the good robustness of this framework, cycling breakthrough experiments demonstrated no capacity loss (Figure 6c and S38).

As an important factor, large-scale preparation of porous adsorbents has received widespread attention. The preparation of **NTU-88** on a large-scale (≈60 g) has been achieved by a string the corresponding ligand and metal ion in solution for only 1 min with the addition of ammonia at room temperature (Figure 6d). Obviously, this facile preparation can be scaled up to kilogram-level production. The phase purity of the microcrystals prepared on a large-scale was confirmed by PXRD analysis, and their stability was demonstrated by maintaining the same diffraction pattern even after being exposed to air for a duration of 11 months

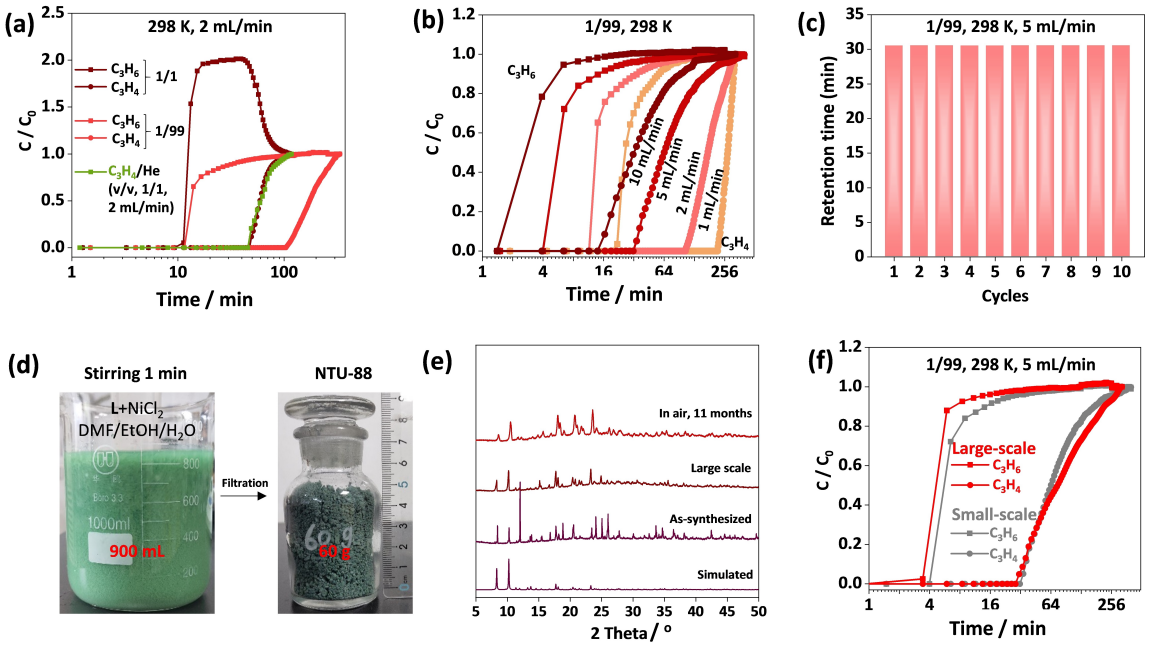

Figure 6. Experimental breakthrough curves of **NTU-88** for C_3H_4/C_3H_6 and C_3H_4/He (a); breakthrough curves of **NTU-88** for C_3H_4/C_3H_6 at different velocities (b); cycling breakthrough curves of **NTU-88** for C_3H_4/C_3H_6 (c); photos of the large-scale synthesis (d); PXRD of **NTU-88** (e); breakthrough curves of large-scale and small-scale synthesized **NTU-88** (f). All experiments were conducted at a pressure of 1 bar.

(Figure 6e). Meanwhile, the porosity and the function of the confined-rotational shutters were validated through static C_3H_4 and C_3H_6 adsorption isotherms, as well as the dynamic breakthrough experiments (Figure 6f and S45).

Conclusion

On the demand of highly pure C_3H_6, we here report a soft crystal with a confined-rotational shutter that can effectively sieve C_3H_4/C_3H_6 mixtures. The rotated pyridine ring in the nanospace creates a maximum aperture of 4.4 Å that allows exclusive C_3H_4 adsorption, but not C_3H_6. With a record high uptake ratio, good capacity, scalable synthesis and good stability, **NTU-88** holds great potential for feasible C_3H_4/C_3H_6 separation. Furthermore, the identification of transition structures during gas-induced phase change greatly enhances our comprehension of the pore-gating effect in flexible structure-types. Moving forward, this strategy has high potential to be extended to future analogues, thereby creating an important opportunity to develop optimized materials for challenging separations with high capacity and no co-adsorption.

Supporting Information

The single crystal diffraction data for NTU-88 series were deposited in the Cambridge Crystallographic Data Centre (CCDC) and the deposition numbers are 2266630–2266634.

Acknowledgements

We thank the financial support of the National Natural Science Foundation of China (22171135), the Innovative Research Team Program by the Ministry of Education of China (IRT-17R54) and the National Natural Science Foundation of Jiangsu Provience (BK20231269). K. H. D. thanks Kusunoki 125, PRESTO, Japan Science and Technology Agency Grant No. 22713147, Grant-in-Aids for Scientific Research from Japan Society for the Promotion of Science (KAKENHI) Grant Nos. 20K05419 and 18H05407, and Toyota Mobility Foundation.

Conflict of Interest

The authors declare no conflict of interest.

Data Availability Statement

The data that support the findings of this study are available in the supplementary material of this article.

Keywords: Confined-Rotational Shutters · Gas Separation · Molecular Sieving · Nanoporous Crystals

[1] D. S. Sholl, R. P. Lively, *Nature* **2016**, *532*, 435.
[2] J. C. Santos, A. F. Portugal, F. D. Magalhaes, A. Mendes, *Ind. Eng. Chem. Res.* **2006**, *45*, 1085.
[3] S. Eteve, L. Hay, T. Rottner, US patent, US5223004 A, **1993**.
[4] B. Zhu, L. Li, H. Lin, W. Han, D. Tan, F. Zhang, *Chem. Ind. Eng. Prog.* **2012**, *316*, 1379.
[5] H. Gao, B. Gao, J. Zhang, Z. Yu, *Qilu Petrochem. Technol.* **1999**, *27*, 247.
[6] H. Ma, X. Zhang, X. Zhao, *Pet. Process. Petrochem.* **2004**, *35*, 23.
[7] M. F. Friedrich, M. Lucas, P. Claus, *Catal. Commun.* **2017**, *88*, 73.
[8] H. Furukawa, K. E. Cordova, M. O'Keeffe, O. M. Yaghi, *Science* **2013**, *341*, 1230444.
[9] Y. B. Zhang, H. L. Zhou, R. B. Lin, C. Zhang, J. B. Lin, J. P. Zhang, X. M. Chen, *Nat. Commun.* **2012**, *3*, 1654.
[10] S. H. Yang, A. J. Ramirez-Cuesta, R. Newby, V. Garcia-Sakai, P. Manuel, S. K. Callear, S. I. Campbell, C. C. Tang, M. Schroder, *Nat. Chem.* **2015**, *7*, 121.
[11] J. W. Yoon, H. Chang, S. J. Lee, Y. K. Hwang, D. Y. Hong, S. K. Lee, J. S. Lee, S. Jang, T. U. Yoon, K. Kwac, Y. Jung, R. S. Pillai, F. Faucher, A. Vimont, M. Daturi, G. Ferey, C. Serre, G. Maurin, Y. S. Bae, J. S. Chang, *Nat. Mater.* **2017**, *16*, 526.
[12] C. Gu, N. Hosono, J. J. Zheng, Y. Sato, S. Kusaka, S. Sakaki, S. Kitagawa, *Science* **2019**, *363*, 387.
[13] H. Z. Wang, Z. L. Shi, J. J. Yang, T. Sun, B. Rungtaweevoranit, H. Lyu, Y. B. Zhang, O. M. Yaghi, *Angew. Chem. Int. Ed.* **2021**, *60*, 3417.
[14] P. Q. Liao, N. Y. Huang, W. X. Zhang, J. P. Zhang, X. M. Chen, *Science* **2017**, *356*, 1193.
[15] L. B. Li, R. B. Lin, R. Krishna, H. Li, S. C. Xiang, H. Wu, J. P. Li, W. Zhou, B. L. Chen, *Science* **2018**, *362*, 443.
[16] Z. Shi, Y. Tao, J. Wu, C. Zhang, H. He, L. Long, Y. Lee, T. Li, Y.-B. Zhang, *J. Am. Chem. Soc.* **2020**, *142*, 2750.
[17] A. Cadiau, K. Adil, P. M. Bhatt, Y. Belmabkhout, M. Eddaoudi, *Science* **2016**, *353*, 137.
[18] R. B. Lin, L. B. Li, H. L. Zhou, H. Wu, C. H. He, S. Li, R. Krishna, J. P. Li, W. Zhou, B. L. Chen, *Nat. Mater.* **2018**, *17*, 1128.
[19] V. I. Nikolayenko, D. C. Castell, D. Sensharma, M. Shivanna, L. Loots, K. A. Forrest, C. J. Solanilla-Salinas, K. I. Otake, S. Kitagawa, L. J. Barbour, B. Space, M. J. Zaworotko, *Nat. Chem.* **2023**, *15*, 542.
[20] Z. Chang, D. H. Yang, J. Xu, T. L. Hu, X. H. Bu, *Adv. Mater.* **2015**, *27*, 5432.
[21] B. Le Ouay, S. Kitagawa, T. Uemura, *J. Am. Chem. Soc.* **2017**, *139*, 7886.
[22] G. K. Angeli, E. Loukopoulos, K. Kouvidis, A. Bosveli, C. Tsangarakis, E. Tylianakis, G. Froudakis, P. N. Trikalitis, *J. Am. Chem. Soc.* **2021**, *143*, 10250.
[23] H. Wang, M. Warren, J. Jagiello, S. Jensen, S. K. Ghose, K. Tan, L. Yu, T. J. Emge, T. Thonhauser, J. Li, *J. Am. Chem. Soc.* **2020**, *142*, 20088.
[24] R. B. Lin, L. B. Li, H. Wu, H. Arman, B. Li, R. G. Lin, W. Zhou, B. L. Chen, *J. Am. Chem. Soc.* **2017**, *139*, 8022.
[25] C. M. McGuirk, T. Runcevski, J. Oktawiec, A. Turkiewicz, M. K. Taylor, J. R. Long, *J. Am. Chem. Soc.* **2018**, *140*, 15924.
[26] J. A. Mason, J. Oktawiec, M. K. Taylor, M. R. Hudson, J. Rodriguez, J. E. Bachman, M. I. Gonzalez, A. Cervellino, A. Guagliardi, C. M. Brown, P. L. Llewellyn, N. Masciocchi, J. R. Long, *Nature* **2015**, *527*, 357.
[27] Y. Huang, J. Wan, T. Pan, K. Ge, Y. Guo, J. Duan, J. Bai, W. Jin, S. Kitagawa, *J. Am. Chem. Soc.* **2023**, *145*, 24425.
[28] H. L. Zhou, Y. B. Zhang, J. P. Zhang, X. M. Chen, *Nat. Commun.* **2015**, *6*, 6917.

[29] H. Sato, W. Kosaka, R. Matsuda, A. Hori, Y. Hijikata, R. V. Belosludov, S. Sakaki, M. Takata, S. Kitagawa, *Science* **2014**, *343*, 167.
[30] S. Horike, S. Shimomura, S. Kitagawa, *Nat. Chem.* **2009**, *1*, 695.
[31] S. Q. Ma, D. F. Sun, X. S. Wang, H. C. Zhou, *Angew. Chem. Int. Ed.* **2007**, *46*, 2458.
[32] J. D. Pang, S. Yuan, D. Y. Du, C. Lollar, L. L. Zhang, M. Y. Wu, D. Q. Yuan, H. C. Zhou, M. C. Hong, *Angew. Chem. Int. Ed.* **2017**, *56*, 14622.
[33] Q. Dong, Y. Huang, J. Wan, Z. Lu, Z. Wang, C. Gu, J. Duan, J. Bai, *J. Am. Chem. Soc.* **2023**, *145*, 8043.
[34] Q. Dong, X. Zhang, S. Liu, R. B. Lin, Y. Guo, Y. Ma, A. Yonezu, R. Krishna, G. Liu, J. Duan, R. Matsuda, W. Jin, B. Chen, *Angew. Chem. Int. Ed.* **2020**, *59*, 22756.
[35] Deposition numbers 2266630 (for NTU-88α), 2266631 (for NTU-88o-C_3H_4), 2266632 (for NTU-88c), 2266633 (for NTU-88β) and 2266634 (for NTU-88 as synthesized) contain the supplementary crystallographic data for this paper. These data are provided free of charge by the joint Cambridge Crystallographic Data Centre and Fachinformationszentrum Karlsruhe Access Structures service.

Manuscript received: November 5, 2023
Accepted manuscript online: November 13, 2023
Version of record online: November 27, 2023